PAPER

Check for updates

Human IgG1 Fc pH-dependent optimization from a constant pH molecular dynamics simulation analysis†

Yee Ying Lim, Theam Soon Lim [ID] and Yee Siew Choong [ID] *

The binding of IgG Fc with FcRn enables the long circulating half-life of IgG, where the Fc–FcRn complex interacts in a pH-dependent manner. This complex shows stronger interaction at pH $\leq$ 6.5 and weaker interaction at pH $\geq$ 7.4. The Fc–FcRn binding mechanism that promotes the long circulating half-life of IgG has prompted several IgG Fc-related mutational studies to focus on the pH-dependent Fc–FcRn complex interactions in order to improve the pharmacokinetic properties of Fc. Hence, in this study, we applied the *in silico* constant pH molecular dynamics (CpHMD) simulation approach to evaluate the human Fc–FcRn complex binding (pH 6.0) and dissociating (pH 7.5) mechanism at the molecular level. The analysis showed that the protonated state of the titratable residues changes from pH 6.0 to pH 7.5, where the disrupting energy for Fc–FcRn complex formation was found to be due to the electrostatic repulsion between the complex. According to the analysis, an Fc variant was computationally designed with an improved binding affinity at pH 6.0, which is still able to dissociate at pH 7.5 with FcRn at the *in silico* level. The binding free energy calculation *via* the MMPB/GBSA approach showed that the designed Fc mutant (Mut$_{M4}$) has increased binding affinity only at pH 6.0 compared with the reported mutant (YTE) Fc. This work demonstrates an alternative Fc design with better binding properties for FcRn, which can be useful for future experimental evaluation and validation.

Introduction

Monoclonal antibody (mAb) drugs have remained in a mainstream in the field of medical therapeutics with ∼80 drugs being approved by the Food and Drug Administration (FDA) till date.[1] These mAbs have been used to treat various conditions such as cancer, infectious diseases and autoimmune disorders.[2] Most of the approved mAbs apply full-size immunoglobulin G (IgG), which possesses powerful effector functions found in the full IgG scaffold such as antibody-dependent cellular cytotoxicity (ADCC), antibody-dependent cell-mediated phagocytosis (ADCP) and complementary-dependent cytotoxicity (CDC).[3,4] Besides the aforementioned effector functions, the long *in vivo* serum half-life observed in a few IgG subclasses (IgG1, IgG2 and IgG4)[5] has allowed the advantages of the potential therapeutics design to be conjugated with the effector function-containing IgG crystallisable fragment (Fc) region. This naturally occurring IgG1 has a circulating half-life of ∼21 days due to its low degradation rate, which is related to its escape from lysosomal protein catabolism by binding to the neonatal Fc receptor (FcRn) in a pH-dependent manner.[6,7] The Fc–FcRn interaction is described to be strong at acidic pH ($\leq$6.5) but weaker at neutral pH ($\geq$7.4),[8,9] where the binding of FcRn occurs at the Fc inter-β-sheet loops (CH$_2$:loop$_{AB}$, loop$_{DE}$ and CH$_3$:loop$_{FG}$). A detailed schematic representation of IgG-Fc was described in a review paper.[2] From a biological aspect, an improved Fc–FcRn binding mechanism may contribute to an enhancement in the pharmacokinetics of mAb drugs. The prolonged half-life of designed drugs will encourage lower requirements for administration doses and frequencies.

To date, experimental pH-dependent solved structures are yet to be discovered, hence the *in silico* method can be an alternative approach to study the structural details of the IgG–FcRn complex at the molecular level, *i.e.* evaluation of the pH-dependent binding mechanism of the Fc–FcRn. The overall stoichiometry arrangement of Fc–FcRn complexes was found to be similar in both rodents and humans,[8,10,11] where studies revealed the involvement of the FcRn α1-α2 domain platform interacting with the Fc CH$_2$–CH$_3$ domain interface loops. Engineering studies on IgG1 for FcRn have also been reported,[12–18] with one of the most noteworthy Fc variant, the IgG1 Fc YTE mutant (Met252Tyr, Ser254Thr and Thr256Glu mutations). The IgG1 Fc YTE mutant was reported to show ∼10-fold improved pH-dependent binding affinity whilst exhibiting ∼2 to 4-fold prolonged serum half-life in humans.[14]

Often, the effects of the solvent environment such as pH are key factors in biochemical reactions, including the Fc–FcRn

Institute for Research in Molecular Medicine (INFORMM), Universiti Sains Malaysia, 11800 Minden, Penang, Malaysia. E-mail: yeesiew@usm.my; Tel: +604 653 4801

† Electronic supplementary information (ESI) available. See DOI: 10.1039/c9ra10712f

binding mechanism.[5,11,15,19] Although conventional molecular dynamics (MD) simulation has prompted molecular discovery in biological studies, system settings with a fixed protonation state for solute titratable residues throughout the simulation may hinder the visualization of complex conformational changes in different pH environments. Thus, an auxiliary for MD simulation, constant pH molecular dynamics (CpHMD) simulation, which allows dynamic changes in the protonation states of titratable residues based on changes in the environmental pH was applied in this study. The CpHMD performs dynamic simulation of a system coupled with periodic Monte Carlo (MC) sampling of the protonation states for solute titratable residues. In this study, the simulation trajectories for all systems were further evaluated for their molecular interactions, characterized by the molecular mechanics Poisson–Boltzmann and generalized Born surface area (MMPB/GBSA) approach for binding free energy calculation. The data illustrated the agreement between the binding free energy calculations and the binding trend of other reported experimental results.

Methodology

Generating control complex structures

The initial human Fc–FcRn structure was obtained from the Protein Data Bank (PDB) with 3.80 Å resolution (PDB ID: 4N0U).[8] This X-ray crystallographic structure is comprised of mutant-type IgG1 YTE Fc with three-point mutations (Met252-Tyr, Ser254Thr and Thr256Glu mutation; denoted as Mut_{YTE}). However, the structure of wild-type (WT) human Fc complexed with FcRn is not available. Hence, the WT Fc was manually reverse mutated from Mut_{YTE}. Since Ile253, His310 and His435 were reported to be vital the residues for the FcRn interactions,[20–22] a mutant Fc (Ile253Ala, His310Ala and His435Ala mutations; denoted as Mut_{AAA}) that was mutated from Mut_{YTE} was modelled and used as a counter measure for the non-binding Fc–FcRn complex. The IgG Fc variants (WT and Mut_{AAA}) were modelled using MODELLERv9.21.[23] This work focused on the Fc interactions with the membrane-bound FcRn heavy chain (HC). The non-covalently bound β2-microglobulin (β2m) was excluded from FcRn in all the systems.

Constant pH molecular dynamics (CpHMD) simulation

AMBER18 suite[24] was used for the simulation of all the systems, in accordance with the negative control Mut_{AAA}–FcRn and positive controls WT–FcRn and Mut_{YTE}–FcRc. The residue names for ASP, GLU and HIS were manually changed to AS4, GL4 and HIP to allow them to be detected as titratable residues in all the complexes, respectively. The AMBER ff99SB force field[25] was used to describe the complex and the charges were neutralized by counter ions. Each system was solvated in a truncated TIP3P octahedron water box extended 10 Å from each direction of the solute. All systems were minimized to relieve atomic close contacts of the protein side chains with the solvent by 2000 steps of steepest descent followed by 2000 steps of conjugate gradient method at a constant volume and restraint being set only on protein backbones to ensure

minimal adjustment during minimization. After minimization, the complexes were slowly heated to 300 K within 900 ps using a Langevin thermostat[26] and equilibrated without any restraint for 100 ps. The production stage was performed using CpHMD simulation with Monte Carlo (MC) sampling techniques[27,28] carried out in the pmemd.cuda module on a Dell Precision Tower 5810 equipped with an NVIDIA GeForce GTX 1060 CUDA GPU system. A total of 300 ns CpHMD simulation was performed on each system at pH 6.0 and 7.5, with a 2 fs time step, as implemented in AMBER18. The constant pH setting was turned on for explicit solvent running under the GB_{OBC} model against a salt concentration of 0.1 M (Debye–Hückel based) as a variable control for the binding free energy calculations. The protonation state changing attempts for the titratable residues were set to 3 ps, while the temperature was maintained at 300 K with the Langevin dynamics algorithm with SHAKE algorithm[29] being turned on throughout the simulation. The system was set to retain a constant pressure of 1 atm without imposing any atomic restraints. The particle mesh Ewald (PME) algorithm was used to calculate long range electrostatic interaction and 10 Å as the non-bonded calculation cutoff distance. Representative structures from each system were selected from the clustering of the last 5 ns from all the system trajectories using the kclust binary from MMTSB toolset.[30] Protein stability check including the analysis of root mean square deviation (RMSD), root mean square fluctuation (RMSF) by residues and secondary structure analysis was carried out using the *cpptraj*[31] software incorporated in the AMBER18 software suite. The pK_a calculation, hydrogen bond and binding free energy analysis were performed by taking the median results from a total of 3000 trajectories at (200 ns, 250 ns and 300 ns) intervals of 5 ps as the representative predicted value. The predicted pK_a values for the system titratable residues were obtained from the cpout output file.

Binding free energy calculation and per-residue decomposition

The absolute binding free energies, ΔG_{bind}, for the intermolecular non-covalent interaction of the Fc–FcRn complex was calculated using the molecular mechanics Poisson–Boltzmann and generalized Born surface area (MMPB/GBSA) approaches available in AMBER18 with 1 ns trajectories (1000 snapshots) at 5 ps for each 200 ns, 250 ns and 300 ns, respectively. The ΔG_{bind} for each system was calculated according to (eqn (1)).

$$\Delta G_{bind} = \Delta G_{complex} - (\Delta G_{receptor} + \Delta G_{ligand}) \quad (1)$$

where $\Delta G_{complex}$, $\Delta G_{receptor}$, and ΔG_{ligand} are the free energies of the Fc–FcRn complex, FcRn and Fc, respectively. The difference in free energies (ΔG) for the Fc–FcRn complex, FcRn and Fc in (eqn (1)) was calculated as follows:

$$\Delta G = \Delta E_{MM} + \Delta G_{solvation} - T\Delta S_{conformation} \quad (2)$$

where ΔE_{MM} is the sum of the internal strain energy, also known as the difference in molecular mechanics energy, $\Delta G_{solvation}$ is the solvation free energy, while $T\Delta S_{conformation}$ is the absolute

temperature (in Kelvin), and the vibrational entropy contribution of the complex was calculated using the quasi-harmonic approximation.[32] ΔE_{MM} and $\Delta G_{solvation}$ required for ΔG calculation were obtained from:

$$\Delta E_{MM} = \Delta E_{int} + \Delta E_{vdW} - \Delta E_{ele} \tag{3}$$

$$\Delta E_{int} = \Delta E_{bond} + \Delta E_{angle} - \Delta E_{torsion} \tag{4}$$

$$\Delta G_{solvation} = \Delta G_{polar} + (\gamma \Delta SASA - \beta) \tag{5}$$

where ΔE_{MM} (eqn (3)) is the sum of the molecular energy contribution by bonded (ΔE_{int}), non-bonded van der Waals (ΔE_{vdW}) and electrostatic forces (ΔE_{ele}). ΔE_{int} (eqn (4)) is the molecule internal strain energy calculated from the summation of three energy terms: covalent bonds (ΔE_{bond}), bond angles (ΔE_{angle}) and torsion angles at a single rotation bond ($\Delta E_{torsion}$). $\Delta G_{solvation}$ was calculated based on the summation of the polar (ΔG_{polar}) and non-polar ($\gamma \Delta SASA - \beta$) contribution. The polar (ΔG_{polar}) contribution was solved using the Poisson–Boltzmann (PB) and generalized Born (GB) equation,[33] while the non-polar ($\gamma \Delta SASA - \beta$) contribution was calculated from the solvent-accessible surface area (SASA), which was estimated using fast linear combination of pairwise overlap (LCPO) algorithm.[34] The E_{int} is cancelled out for the G_{bind} calculations as stable energies were obtained from the MD simulations. The binding free energy decomposition was used to analyse the contribution of residues (side chain (ΔT_S) or backbone (ΔT_B)) to the total binding free energy of all systems. By summing up the energy contribution (eqn (2)), the residues that interact in complex formation can be determined. The polar contribution ($\Delta E_{elec+pol}$) was calculated by summation of two energy terms (ΔE_{elec}) and (ΔE_{pol}), whilst the non-polar contribution (ΔE_{vdW+np}) was calculated by energy terms (ΔE_{vdW}) and (ΔE_{np}) summation.

Design of human IgG1 Fc

We used the Mut_{YTE} structure obtained from CpHMD at pH 6.0 as the initial structure for the new Fc variant design, which aimed to further improve the binding with FcRn only in an acidic environment (pH 6.0). In order to improve the binding affinity of Fc for FcRn only at pH 6.0, the complex structure imposed with single-point mutation was obtained based on clustering analysis based on pH 6.0 crystal structure (Mut_{YTE} Fc–FcRn complex) CpHMD simulation system. The Fc interacting residues for FcRn was observed earlier on based on the jsPISA interface analyser,[35] consisting of three loop regions ($CH_{2loop_{AB}}$ residues 249-257, $CH_{2loop_{DE}}$ residues 307-315 and $CH_{3loop_{FG}}$ residues 428-440). Every position in these loop regions were submitted for mutation to 19 alternative amino acids (except His at positions 310 and 435, which were found to be involved in pH-dependent binding mechanism) using the Single Amino Acid Mutation related change of Binding Energy (SAAMBE) web server.[36] The SAAMBE prediction server allows the identification changes in binding free energy upon mutation, where ($\Delta \Delta G$ becomes negative) indicates an improvement in the binding free energy of the complex upon that particular single amino acid mutation. The final combination of single amino acid substitutions into a single

Fc was remodelled using MODELLERv9.21(23). The new Fc design (denoted as Mut_{M4} since it consists of four-mutation points) was then studied using CpHMD simulation. A similar CpHMD system setup was reapplied for the Mut_{M4}–FcRn complex at pH 6.0 and pH 7.5. The results were then compared with that of the earlier mentioned 3 systems (WT–FcRn, Mut_{YTE}–FcRc and Mut_{AAA}–FcRn).

Results

CphMD simulations

In this study, *in silico* prediction utilizing CpHMD was done as an experimental guide to capture the Fc–FcRn complex physicochemical binding property at pH 6.0 and 7.5. The engineering of the IgG Fc region with increased binding affinity for FcRn at pH 6.0 but not pH 7.5 aimed to promote the prolonged therapeutic drug half-life of mAbs or chemical-conjugated Fc drugs based on the biological advantages of IgG1 such as the prolonged serum half-life in humans. This can be viewed as a step to improvise the pharmaco-kinetic properties of Fc-based drug design. Currently, certain therapeutic drugs may be confined by limitations such as complex instability and rapid clearance. Thus, utilizing the Fc–FcRn binding mechanism in Fc-fused drug constructions, in theory may allow its biological advantages to be inherited. Accordingly, by prolonging the drug serum half-life will increase the drug bioavailability, which may benefit patients. Meanwhile, the design of new Fc for FcRn without compromising the pH-dependent binding mechanism remains a challenge in Fc engineering procedures. Thereby, this study modelled a new Fc mutant (Mut_{M4}) by mutating the Fc residues found interacting with FcRn to 19 alternative amino acids using the SAMMBE prediction server. The resulting Mut_{M4} (Asp249Ala, Thr254Phe, Pro257Trp and Asp312Gly) was designed, which showed that Asp249Ala, Thr254Phe, Pro257Trp and Asp312Gly show improve binding affinity ($\Delta \Delta G_{Mut}$) for FcRn (ESI, Fig. S1†). The Fc–FcRn interacting residues are located at the Fc (CH_2-loop$_{AB}$: 244-257; CH_2-loop$_{DE}$: 308-318; and CH_3-loop$_{FG}$: 429-435) and FcRn heavy chain (loop$_{\alpha'1-\beta'C}$: 82-89; loop$_{\beta'DE}$: 112-115; and loop$_{\beta'G-\alpha'2}$: 129-133) (ESI Fig. S2†). The designed Mut_{M4}–FcRn complex was subjected to simulation, resulting in a total of four Fc mutations complexed with FcRn (Table 1). RMSD analysis showed that while approaching 300 ns, the Fc–FcRn complex backbone carries a trajectory convergence with a lower RMSD (max of ~5 Å and min of ~2 Å) at pH 6.0 compared to that at pH 7.5 (max of ~8 Å and min of ~2 Å) (Fig. 1). In each system, the structure falling in the major cluster with the closest centroid mass RMSD from the last 5 ns trajectories was selected as the representative structure of the system. The selected structures were used for comparison with the available crystal structure (PDB_ID: 4NOU), showing that the complexes at pH 6.0 are more similar to the crystal structure (ESI Fig. S3†). The extracted trajectories from all systems were compared among each other and showed higher quaternary conformational changes at pH 7.5 (Fig. 2). Noticeably, FcRn showed a positional shift in Mut_{YTE}–FcRn and Mut_{M4}–FcRn in the two different pH environments compare with WT–FcRN and Mut_{AAA}–FcRn. The final recorded RMSD difference between the

Table 1 Interacting residues of IgG1-Fc region for FcRn. The underlines denote the mutant residues

Fc variant	CH$_{2(\text{loop}_{AB})}$	CH$_{2(\text{loop}_{DE})}$	CH$_{3(\text{loop}_{FG})}$
Residue number	249-257	307-315	428-440
AAA-mutant (Mut$_{AAA}$)	DTLM<u>A</u>SRTP	TVL<u>A</u>QDWLN	MHEALHN<u>A</u>YTQKS
Wildtype (WT)	DTLMISRTP	TVLHQDWLN	MHEALHNHYTQKS
YTE-mutant (Mut$_{YTE}$)	DTL<u>Y</u>IT<u>R</u>E<u>P</u>	TVLHQDWLN	MHEALHNHYTQKS
M4-mutant (Mut$_{M4}$)	<u>A</u>TLYIF<u>REW</u>	TVLHQ<u>G</u>WLN	MHEALHNHYTQKS

representative structures was 3.7 Å, 1.6 Å, 6.0 Å, and 4.6 Å for Mut$_{AAA}$–FcRn, WT–FcRn, Mut$_{YTE}$–FcRn and Mut$_{M4}$–FcRn, respectively, with no major secondary structure changes observed in the individual Fc and FcRn at either pH 6.0 or pH 7.5 for all systems (ESI, Fig. S4†).

Fc domain interface mutation induced shifts in Fc–FcRn complex binding affinity

MMPB/GBSA approach binding free energy calculation taking the average binding free energy from 200 ns, 250 ns and 300 ns with each 1000 trajectories at 5 ps intervals was carried out

(resulting in 200 trajectories in each nanosecond, and a total of 600 trajectories to be used in the calculation). Fig. 3 presents the average binding energy contributions of all the complexes. Compared to the Fc variants at pH 6 (red bars), ΔG_{bind} showed an increase for all the Fc variants against FcRn at pH 7.5 (yellow bars), indicating the loss in binding affinity for the Fc–FcRn complexes at higher pH. MMGBSA predicted the difference in binding affinity ($\Delta\Delta G_{\text{bind}}$) between Mut$_{YTE}$ and WT to be -3.58 kcal mol^{-1} and $+2.14$ kcal mol^{-1} at pH 6.0 and pH 7.5, while the difference in $\Delta\Delta G_{\text{bind}}$ between Mut$_{M4}$ and WT to be -4.15 kcal mol^{-1} and $+0.52$ kcal mol^{-1} at pH 6.0 and pH 7.5, respectively, indicating the improved binding of Mut$_{M4}$ over Mut$_{YTE}$ for FcRn at pH 6.0 ($\Delta\Delta G_{\text{bind}}$ of -0.56 kcal mol^{-1}) with dissociating potential. Similarly, the MMPBSA calculation predicted the difference in $\Delta\Delta G_{\text{bind}}$ between Mut$_{YTE}$ and WT to be -1.61 kcal mol^{-1} and -5.87 kcal mol^{-1} at pH 6.0 and pH 7.5, respectively, while the difference in $\Delta\Delta G_{\text{bind}}$ between Mut$_{M4}$ and WT to be -6.46 kcal mol^{-1} and -4.23 kcal mol^{-1} at pH 6.0 and pH 7.5, respectively, indicating an improved binding of Mut$_{M4}$ over Mut$_{YTE}$ for FcRn at pH 6.0 ($\Delta\Delta G_{\text{bind}}$ of -4.85 kcal mol^{-1}).

The non-polar interaction was analyzed based on the summation of the van der Waals and non-polar contribution ($\Delta E_{\text{vdW+np}}$), while electrostatic interaction and hydrogen bonding was analyzed based on the summation of the
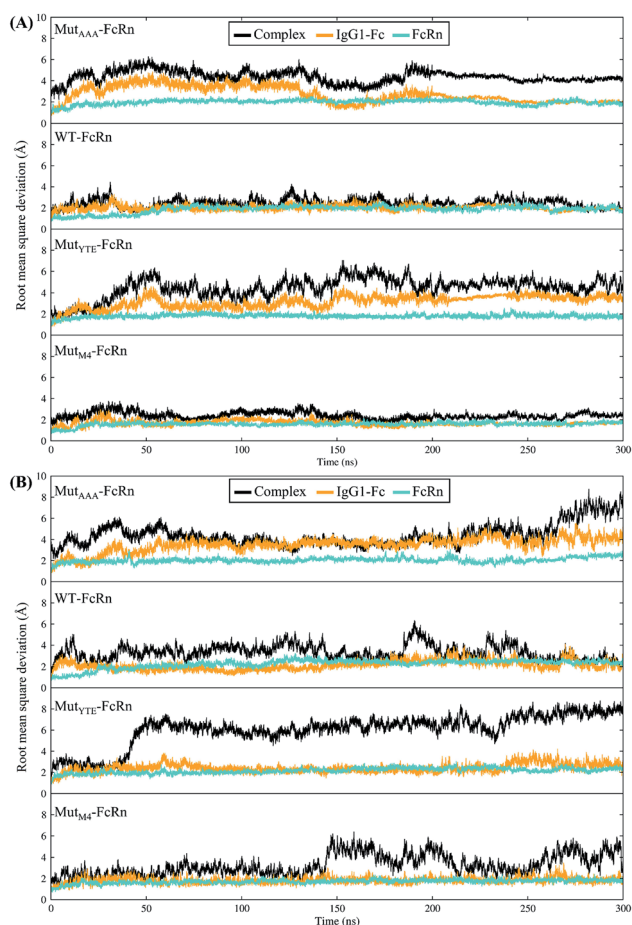

Fig. 1 Root mean square deviation of the backbone atoms (RMSD$_{\text{C}\alpha,\text{N,C,O}}$) with the function of time at (A) pH 6.0 and (B) pH 7.5 for Fc Mut$_{AAA}$, WT, Mut$_{YT}$E and Mut$_{M4}$, respectively, in the complex with FcRn.
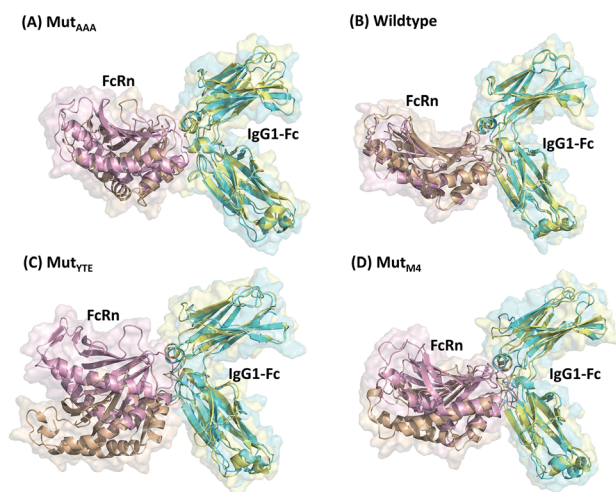

Fig. 2 Superimposition of (A) Mut$_{AAA}$–FcRn, (B) WT–FcRn, (C) Mut$_{YTE}$–FcRn, and (D) Mut$_{M4}$–FcRn complexes at pH 6.0 (Fc: cyan and FcRn: pink ribbon presentation) and pH 7.5 (Fc: yellow & FcRn: orange ribbon presentation). Figure was prepared using Pymol.[37]
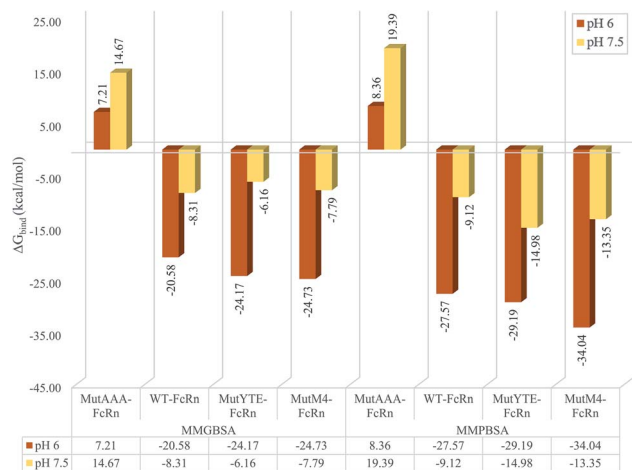
Fig. 3 Bar chart demonstrating the Fc−FcRn complex average binding free energy (ΔG_{bind}) calculated using MMGBSA (left four columns) and MMPBSA (right four columns) for Mut_{AAA}−FcRn, WT−FcRn, Mut_{YTE}−FcRn, and Mut_{M4}−FcRn complexes at pH 6.0 (red) and pH 7.5 (yellow).

electrostatic and polar contribution ($\Delta E_{elec+polar}$). Regardless of the pH value, all the complexes were shown to be stabilized with non-polar interactions (ΔE_{vdW+np}) in the sequence of binding affinity ranked from high to low as follows: Mut_{YTE} > Mut_{M4} > WT > Mut_{AAA} at pH 6.0 and Mut_{M4} > Mut_{YTE} > WT > Mut_{AAA} at pH 7.5 (Fig. 4 blue (pH 6) and pink (pH 7.5) bars). The pair-wise decomposition energies involved in complex formation are listed in ESI, Table S1† (MMGBSA) and Table S2† (MMPBSA). In addition to the interacting residues listed based on the MMPB/GBSA calculation, representing structures were analyzed for close contacts in the Fc−FcRn complexes (ESI, Table S3†).

Along with aforementioned interaction analysis, hydrogen bond frequency was examined from the trajectories used in the $\Delta \Delta G_{bind}$ calculations. Table 2 provides information on the hydrogen bonding that occurred > 50% of the extracted simulation time between Fc and FcRn at pH 6.0 and pH 7.5, which

Fig. 4 Bar chart demonstrating the hydrophilic ($\Delta E_{elec+polar}$) and hydrophobic interaction (ΔE_{vdW+np}) calculated using MMGBSA (left four columns) and MMPBSA (right four columns) for the Mut_{AAA}−FcRn, WT−FcRn, Mut_{YTE}−FcRn, and Mut_{M4}−FcRn complexes at pH 6.0 (black and blue bars) and pH 7.5 (blue and pink bars).

identified that the higher binding affinity of Mut_{YTE}−FcRn over WT at pH 6.0 is probably due to the stronger hydrogen bonds (higher percentage of occupancies) involved in complex formation. Besides, the decomposition $\Delta \Delta G_{bind}$ also revealed sizeable interactions between the spatially adjacent residues in the complex related to stronger electrostatic interactions and hydrogen bonding at pH 6.0. If the Fc−FcRn complexes were to be drawn closer, an increase in core hydrophobic interactions is likely to occur. In contrast, most of the electrostatic interactions were unstable and did not achieve 50% occupancy of the extracted trajectories. It was observed that His310 (Fc) lost its hydrogen bond interaction with Glu115 (FcRn) at pH 7.5. With the chemical property of His to naturally performs protonation state fluctuations around pH 6.6, it was predicted that a basic pH will cause the His residue to be deprotonated and end up with a net neutral charge. Overall, this will reduce the electrostatic interaction between Fc and FcRn by hydrogen bond deformation, and hence, can be used to explain the release of IgG1 Fc from FcRn at pH 7.5. Despite the loss of the Fc:FcRn (His310:Glu115) hydrogen bond interaction, Fc:FcRn (Ser254:Glu133) contact remained at both pH 6 and 7.5. This can explain why there is still a binding affinity for WT−, Mut_{YTE}− and Mut_{M4}−Fc with FcRn at pH 7.5 and can possibly cause the slow release of Fc from the complex at higher pH. The Fc−FcRn interaction figures were depicted. The interacting residues were pooled from pairwise decomposition energy, structure and hydrogen bond analysis. The observed interactions in each system at both pH are depicted in Fig. 5 and 6, respectively. Generally, the results show a reduction in the number of favorable interacting residues at pH 7.5.

Protonation states of titratable residues

Overall, there are ~100 titratable residues for the four complexes (~52 acidic and ~48 basic titratable residues). Table 3 lists the predicted pK_a values predicted by *cpstats* (AMBER18) for the acidic titratable residues resides on the Fc−FcRn complex interface. The theoretical pK_a values were calculated using Delphi pK_a prediction[38] by submitting a single trajectory complex structure utilizing the AMBER force field. Delphi pK_a prediction was performed on the crystal structures and representative structures from all the simulation systems. However, only the *cpstats* pK_a prediction results for interacting titratable residues of all simulation systems are presented since they show observable pK_a shifts. The pK_a value deviated from the reference value (predicted by Delphi) under the circumstances of interaction with neighboring residues. For instance, considering that His310 (reference pK_a: 6.6) showed lower predicted pK_a values, the residue needs a lower pH environment to be protonated. This can be related to the electronegative atoms of the residue, which is constantly involved in hydrogen bonding with its neighboring residues. This leads to difficulty in accepting additional protons, hence decreasing the predicted pK_a value. The pK_a prediction from the Delphi program showed similar results for all the submitted structures as the program rebuilt the environment for solute pK_a prediction and is insufficient to provide an observable correlation between the
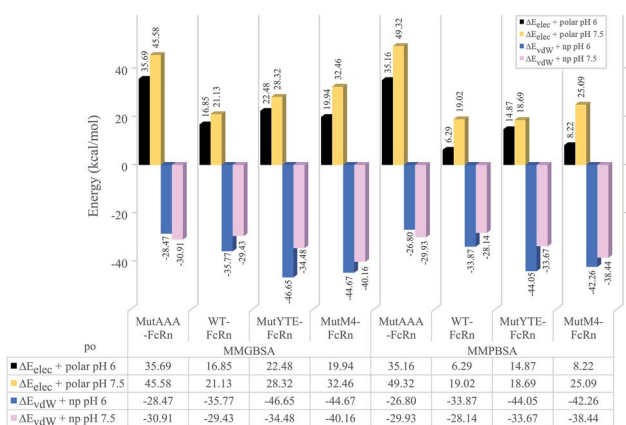
Table 2 Hydrogen bonds formed between Fc and FcRn at pH 6.0 and pH 7.5. Only hydrogen bonds occurring >50% are reported. Bold residues are the titratable residues

	pH 6.0					pH 7.5				
	IgG1-Fc	FcRn	Occupancies (%)	Average distance (Å)	Average angle (°)	IgG1-Fc	FcRn	Occupancies (%)	Average distance (Å)	Average angle (°)
Mut$_{AAA}$	Ser254$_{HG}$	Glu133$_{OE1}$	96.5	2.7	165.0	Asn434$_{H}$	Asp130$_{O}$	72.4	2.8	155.1
	Gln311$_{H}$	Glu115$_{OE1}$	64.8	2.9	161.2	—	—	—	—	—
WT	Ser254$_{HG}$	Glu133$_{OE2}$	99.0	2.7	165.6	Ser254$_{H}$	Glu133$_{OE2}$	65.7	2.9	159.7
	His310$_{HD1}$	Glu115$_{OE2}$	80.7	2.8	159.2	—	—	—	—	—
	Leu253$_{O}$	Asn113$_{HD22}$	65.2	2.9	160.0	—	—	—	—	—
Mut$_{YTE}$	Thr254$_{OG1}$	Glu133$_{HE11}$	95.0	2.7	165.9	—	—	—	—	—
	His310$_{ND1}$	Glu115$_{HE12}$	88.3	2.8	162.6	Thr254$_{HG1}$	Glu133$_{OE2}$	61.3	2.7	165.8
	His435$_{HD1}$	Asp130$_{O}$	83.9	2.8	158.9	—	—	—	—	—
Mut$_{M4}$	His310$_{HD1}$	Glu115$_{OE1}$	92.9	2.8	154.1	Phe254$_{H}$	Glu133$_{OE2}$	59.5	2.9	155.8
	Gln311$_{HE22}$	Glu116$_{O}$	85.0	2.8	162.0	—	—	—	—	—
	Ile253$_{H}$	Glu133$_{OE1}$	55.9	2.9	158.0	—	—	—	—	—
	Phe254$_{H}$	Glu133$_{OE2}$	54.9	2.9	161.7	—	—	—	—	—

quaternary complex changes and difference in the respective pK_a values (data not presented). Albeit, the following point can be deduced from the pK_a results of both the Delphi and *cphstats* pK_a prediction. The aforementioned His310, which is important in Fc–FcRn complex formation, can have a trapped hydrogen atom that hovers between His310 (Fc) and Glu115 (FcRn).

Under the influence of mutations in the neighbor loop (CH$_{2loop_{AB}}$), an extreme protonation state can be seen between Fc:FcRn (His310:Glu115) at pH 6, indicating there is a stronger hydrogen bond between both residues. This result agrees with the hydrogen bond analysis. Referring to the protonation fraction of both residues, FcRn (Glu115) acts as a hydrogen donor in the Mut$_{YTE}$–FcRn complex while a hydrogen acceptor in the
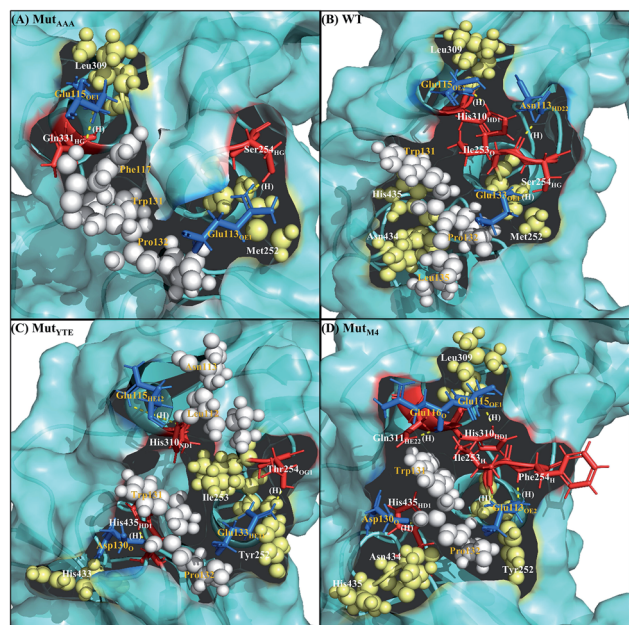

Fig. 5 Interaction interfaces of (A) Mut$_{AAA}$, (B) WT, (C) Mut$_{YTE}$, and (D) Mut$_{M4}$ with FcRn at pH 6.0. IgG1-Fc residues involved in electrostatic interaction are displayed as red sticks, while the FcRn residues involved in electrostatic interactions are displayed as blue sticks. IgG1-Fc residues involved in hydrophobic interactions are displayed as yellow spheres, while FcRn residues involved in hydrophobic interactions are displayed as white spheres. Yellow dots labelled with (H) are the hydrogen bonds between Fc and FcRn. Figure was prepared using Pymol.[37]

Fig. 6 Interaction interface of (A) Mut$_{AAA}$, (B) WT, (C) Mut$_{YTE}$, and (D) Mut$_{M4}$ with FcRn at pH 7.5. IgG1-Fc residues involved in electrostatic interactions are displayed as red sticks, while FcRn residues involved in electrostatic interactions are displayed as blue sticks. IgG1-Fc residues involved in hydrophobic interactions are displayed as teal spheres, while FcRn residues involved in hydrophobic interactions are displayed as white spheres. Yellow dots labelled with (H) are the hydrogen bonds between Fc and FcRn. Figure was prepared using Pymol.[37]
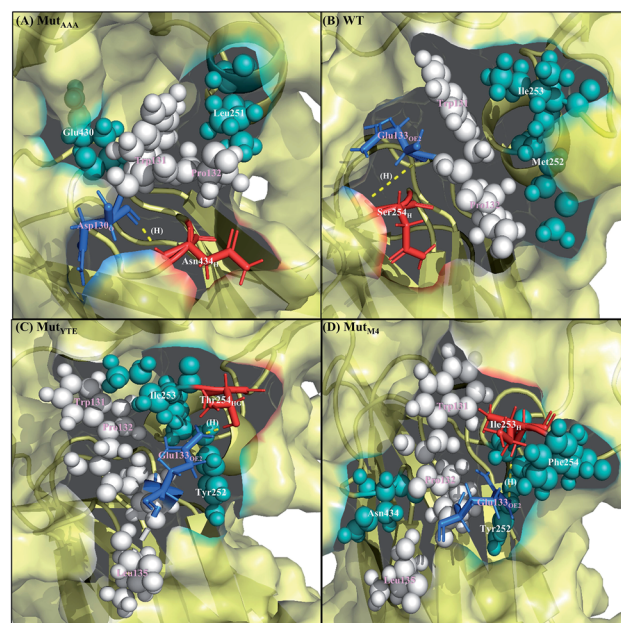
Table 3 The average pK_a value from 200 ns, 250 ns and 300 ns of Fc–FcRn complex titratable interacting residues[a]

| | | Predicted pK_a | | | | | | | | | Protonation fraction | | | | | | | |
| | | pH 6.0 | | | | | pH 7.5 | | | | pH 6.0 | | | | pH 7.5 | | | |
		Crystal	Mut$_{AAA}$	WT	Mut$_{YTE}$	Mut$_{M4}$	Mut$_{AAA}$	WT	Mut$_{YTE}$	Mut$_{M4}$	Mut$_{AAA}$	WT	Mut$_{YTE}$	Mut$_{M4}$	Mut$_{AAA}$	WT	Mut$_{YTE}$	Mut$_{M4}$
Fc	His310	7.99	Null	6.12	3.99	$-\infty$	Null	6.96	5.99	6.53	Null	42.5	2.9	67.3	Null	49.2	40.8	22.9
	His433	6.98	5.91	5.85	6.85	5.80	6.86	5.78	4.18	5.95	45.8	41.8	86.0	39.0	19.6	7.2	0.2	3.5
	His435	6.61	Null	7.79	4.81	8.83	Null	8.51	9.05	9.17	Null	98.2	100.0	99.8	Null	95.3	97.2	97.7
FcRn	Glu115	2.41	7.85	5.90	6.48	3.70	6.66	6.97	5.80	6.18	97.7	64.4	70.0	0.4	26.7	47.8	2.0	8.5
	Glu116	3.23	5.24	4.67	4.24	4.30	5.42	5.06	4.34	4.75	15.3	7.0	2.8	2.0	6.8	8.0	0.2	0.2
	Asp130	3.15	5.69	4.73	4.21	3.89	5.35	5.50	5.34	5.02	35.3	6.7	1.7	0.8	11.2	10.3	0.7	0.3
	Glu133	2.45	1.60	$-\infty$	5.23	2.48	6.61	4.76	4.10	3.40	33.3	0.0	43.3	0.0	20.5	7.6	0.0	0.0

[a] Crystal structure: (PDB ID: 4N0U).

Mut$_{M4}$–FcRn complex. In contrast, WT–Fc, which binds with lower affinity compared to Mut$_{YTE}$ and Mut$_{M4}$, shows an equal distribution of protonation fractions between both residues at pH 6. Meanwhile, Mut$_{AAA}$ with the absence of Fc His310 causes FcRn Glu115 to take up the solvent hydrogen, leading to an increase in its pK_a value at pH 6. The property of Fc His310 seems essential for Fc–FcRn formation. This was observed in the WT–FcRn complex at pH 6, where the Fc His 310 pK_a value is close to its reference pK_a value, while the high pK_a in Glu115 (FcRn) (pK_a: 5.9) indicates less stable hydrogen bond formation. A similar pK_a value was found at pH 7.5 for WT, Mut$_{YTE}$ and Mut$_{M4}$–FcRn, which shows the loss in this interaction is sufficient to cause complex dissociation at higher pH. Overall, the pK_a values agree with the calculated hydrogen bond occupancies.

Discussion

This study applied CpHMD, which allowed the study of the Fc and FcRn pH-dependent binding mechanism. Since the major pH-dependent interacting surface was found in the reside between the FcRn heavy chain and the Fc region, the use of CpHMD simulation was expected to capture the complex quaternary configuration changes at different pH, namely pH 6.0 and pH 7.5. The simulation study showed that the performance of monomeric Fc with FcRn does not lose the pH-dependent binding mechanism, where monomeric Fc was employed for all the simulation systems.[39–43] All the systems showed some degree of conformation rearrangement, with a greater extent observed at pH 7.5 (Fig. 1 and ESI Fig. S2†). However, the lower RMSD at pH 6.0 can possibly be due to the closer pH environment when the crystal structure is obtained (pH 5.2). All the complexes (WT–FcRn, Mut$_{AAA}$–FcRn, Mut$_{YTE}$–FcRn and Mut$_{M4}$–FcRn) showed higher stability at pH 6.0 with an average RMSD of 1.0 Å, 0.4 Å 3.2 Å and 2.3 Å, respectively. The low RMSD values of Mut$_{AAA}$–FcRn for both pH was expected since this Fc variant has been proven to lose its binding capability for FcRn at both pH 6.0 and pH 7.5 (Kim *et al.*, 1994).[44] Hence, it was expected that the Mut$_{AAA}$ binding with FcRn at pH 6.0 and 7.5 should show less significant quaternary structural

deviation. The analysis of the RMSD demonstrated that Mut$_{YTE}$ and Mut$_{M4}$ variant complexes at pH 7.5 exhibited a higher RMSD value. Further analysis from the superimposition of the complex structures at pH 6.0 and 7.5 revealed that not all the quaternary complexes showed obvious detachment of FcRn from the IgG1-Fc interface (FcRn moving downwards from the Fc region was only observed in Mut$_{YTE}$ and Mut$_{M4}$) (Fig. 2). Analysis of the distance between Fc Thr307 and Val427 with FcRn Thr89 showed that only Mut$_{YTE}$ and Mut$_{M4}$ have a greater distance from FcRn at pH 7.5 (ESI, Fig. S5†). For instance, an increased in the distance between FcRn Thr89 and Fc Thr307 from ∼18 Å to ∼24 Å was observed in these two mutants (Mut$_{YTE}$ and Mut$_{M4}$) at pH 7.5, while the others (WT and Mut$_{AAA}$) maintained a similar distance with FcRn (ESI, Fig. S6†). Both the backbone and distance RMSD information led to the conjecture of the importance of the Fc residues at positions 252, 254 and 256 as the mutations resulted in observable posture changes in the Fc–FcRn complex at pH 6.0 and pH 7.5. Since the structural superimposition did not show the total detachment of Fc–FcRn, the Fc–FcRn binding affinity at pH 6.0 and pH 7.5 was further calculated by applying physical principles to explain their molecular interactions. The predicted binding energies are consistent with the reported experimental data,[11,17,45] with the binding affinity following the order of Mut$_{YTE}$ > WT > Mut$_{AAA}$ (Fig. 3). Despite the absence of the FcRn light chain (β2-microglobulin), Mut$_{YTE}$, which was reported to show an increased IgG serum half-life and binding affinity at pH 6.0 compared to WT,[8,46] and thus our calculated total binding energy is agreement with the binding trend of the reported results.

In nature, changes in the His protonation states occur at around pH 6.6, which is within the range of this study. The pK_a prediction results (Table 3) showed that three His residues are supposed to be protonated at pH 6.0 with the side chain being positively charged whilst deprotonation should occur at pH 7.5, which carries a neutral net charge. Compared to the crystal structure, the CpHMD simulation systems show lower predicted pK_a values for Fc His310 and His433 at both pH 6.0 and pH 7.5 (Table 3). His433 showed hydrophobic interaction with FcRn Asp130 in some variants (Mut$_{AAA}$ and Mut$_{M4}$). The positively

charged Fc His433 and His435 with the negatively charged FcRn Asp130 and Glu133 also contributed to Fc–FcRn complex formation at pH 6.0. Supposedly, at pH 7.5, Fc His433 and His435 are neutral, while FcRn Asp130 and Glu133 remain negatively charged, thus leading to the loss of binding interactions with Fc. However, only His433 showed deprotonation at pH 7.5, while His435 remained highly protonated, suggesting this is the cause of the favorable binding free energy calculated at pH 7.5. His433 showed lower pK_a values, while His435 showed a higher pK_a value, which is caused by the competition between neighboring residues. The His residue in solution carries a pK_a of around 6.6, but the value can vary widely from 3 to 9 depending on its burial position or polar and ionic interaction with the neighboring residues.[47] Accordingly, an inconsistent pK_a value calculation can occur in the presence of close interactions with neighboring residues, as described in the literature.[48,49] Both residues can be competing for protonation with the favorable protonation position in His435, as evidenced by the high protonation fraction of His435, whilst His433 showed a drastic decrease in protonation fraction at pH 7.5 for the all variants. Another inconsistent pK_a value was observed for IgG1-Fc His310, which was found to have consistent involvement in electrostatic interactions or hydrogen bonding with FcRn Glu115, in agreement with a report stating the importance of the His310 in complex formation with FcRn.[8] The per residue decomposition of binding free energies (ESI, Table S1†) and hydrogen bond analysis (Table 2) predicted the consistent presence of Fc–FcRn interactions as Fc:FcRn: (His310:Glu115; Ser/Thr254:Glu133), indicating the importance of these four residues in Fc–FcRn complex formation.

The design of the new Fc mutant was aimed to further improve Mut$_{YTE}$ without interfering with the important pH-dependent residues, e.g. His310, at pH 6.0, but able to dissociate at pH 7.5. The Mut$_{M4}$ design showed higher binding affinity with FcRn at pH 6.0 in both MMPB/GBSA calculation with the average binding free energy ($\Delta G_{bind\_PB} = -34.04 \pm 0.66$ kcal mol^{-1}; $\Delta G_{bind\_GB} = -24.73 \pm 0.46$ kcal mol^{-1}) compared with Mut$_{YTE}$ ($\Delta G_{bind\_PB} = -29.19 \pm 0.97$ kcal mol^{-1}; $\Delta G_{bind\_GB} = -24.17 \pm 0.79$ kcal mol^{-1}) and the reduced binding affinity at pH 7.5 ($\Delta G_{bind\_PB} = -13.35 \pm 0.62$ kcal mol^{-1}; $\Delta G_{bind\_GB} = -7.79 \pm 0.46$ kcal mol^{-1}), which is close to Mut$_{YTE}$ ($\Delta G_{bind\_PB} = -14.98 \pm 0.72$ kcal mol^{-1}; $\Delta G_{bind\_GB} = -6.16 \pm 0.66$ kcal mol^{-1}) at pH 7.5. The improved binding affinity of Mut$_{M4}$ compared with Mut$_{YTE}$ at pH 6.0 ($\Delta G_{bind\_PB} = -4.85$; $\Delta G_{bind\_GB} = -0.56$ kcal mol^{-1}) can be attributed to the reduction in the negative repulsion (Asp249Ala and Asp312Gly) and improvement in the non-polar interaction (Ser254Phe and Pro257Trp) with FcRn. Meanwhile, the efficient dissociation of Mut$_{M4}$ from FcRn at pH 7.5 is attributed to the same repulsive mechanism between Fc His433 and His435 with FcRn Asp130 and Glu133, as mentioned earlier.

Conclusions

The pH-dependent binding mechanism of IgG–FcRn allows prolonged IgG serum half-lives of up to ~21 days by efficient binding with the neonatal Fc receptor at acidic pH (pH 6.0) and dissociation at physiological pH (pH 7.5). Without the successful dissociation of IgG from the receptor at physiological pH, the rate of biomolecule catabolism will be increased. The application of the constant pH MD simulation method allowed the changes in the protonation states of the Fc–FcRn titratable residues at the interacting interface to be identified. We then applied the available structural knowledge to design an *in silico* Fc variant, namely Mut$_{M4}$, which can associate and dissociate at the respective pH. This application can be a useful step to optimize the pharmacokinetics of therapeutic molecules, and thus provide more designs for therapeutic molecules for future validation.

Funding

Conflicts of interest

There are no conflicts to be declared.

Acknowledgements

References

1 G. L. Kumar, FDA-Approved Targeted Therapies in Oncology, *Predictive Biomarkers in Oncology*, 2019, pp. 605–622.

2 E. Lobner, M. W. Traxlmayr, C. Obinger and C. Hasenhindl, Engineered IgG1-Fc – one fragment to bind them all, *Immunol. Rev.*, 2016, **270**(1), 113–131.

3 M. D. Hulett and P. M. Hogarth, Molecular basis of Fc receptor function, *Advances in Immunology*, Elsevier, 1994, vol. 57, pp. 1–127.

4 F. Nimmerjahn and J. V. Ravetch, Fcγ receptors as regulators of immune responses, *Nat. Rev. Immunol.*, 2008, **8**(1), 34–47.

5 D. C. Roopenian and S. Akilesh, FcRn: the neonatal Fc receptor comes of age, *Nat. Rev. Immunol.*, 2007, 7(9), 715.

6 C. Chaudhury, S. Mehnaz, J. M. Robinson, W. L. Hayton, D. K. Pearl, D. C. Roopenian, *et al.*, The major histocompatibility complex–related Fc receptor for IgG (FcRn) binds albumin and prolongs its lifespan, *J. Exp. Med.*, 2003, **197**(3), 315–322.

7 V. Ghetie and E. S. Ward, Multiple roles for the major histocompatibility complex class I–related receptor FcRn, *Annu. Rev. Immunol.*, 2000, **18**(1), 739–766.

8 V. Oganesyan, M. M. Damschroder, K. E. Cook, Q. Li, C. Gao, H. Wu, *et al.*, Structural insights into neonatal Fc receptor-based recycling mechanisms, *J. Biol. Chem.*, 2014, **289**(11), 7812–7824.

9 M. Raghavan, V. R. Bonagura, S. L. Morrison and P. J. Bjorkman, Analysis of the pH dependence of the neonatal Fc receptor/immunoglobulin G interaction using

antibody and receptor variants, *Biochemistry*, 1995, **34**(45), 14649–14657.

10 W. P. Burmeister, A. H. Huber and P. J. Bjorkman, Crystal structure of the complex of rat neonatal Fc receptor with Fc, *Nature*, 1994, **372**(6504), 379.

11 W. L. Martin, A. P. West Jr, L. Gan and P. J. Bjorkman, Crystal structure at 2.8 Å of an FcRn/heterodimeric Fc complex: mechanism of pH-dependent binding, *Mol. Cell*, 2001, **7**(4), 867–877.

12 L. G. Presta, R. L. Shields, A. K. Namenuk, K. Hong and Y. G. Meng, Engineering therapeutic antibodies for improved function, *Biochem. Soc. Trans.*, 2002, **30**(4), 487–490.

13 X. Wang, M. Mathieu and R. J. Brezski, IgG Fc engineering to modulate antibody effector functions, *Protein Cell*, 2018, **9**(1), 63–73.

14 W. F. Dall'Acqua, P. A. Kiener and H. Wu, Properties of human IgG1s engineered for enhanced binding to the neonatal Fc receptor (FcRn), *J. Biol. Chem.*, 2006, **281**(33), 23514–23524.

15 A. Saxena, B. Bai, S. C. Hou, L. Jiang, T. Ying, S. Miersch, *et al.*, Fc engineering: Tailored synthetic human IgG1-Fc repertoire for high-affinity interaction with FcRn at pH 6.0, *Methods Mol. Biol.*, 2018, **1827**, 399–417.

16 A. Saxena and D. Wu, Advances in therapeutic Fc engineering - modulation of IgG-associated effector functions and serum half-life, *Front. Immunol.*, 2016, **7**, 580.

17 M. J. Borrok, Y. Wu, N. Beyaz, X. Q. Yu, V. Oganesyan, W. F. Dall'Acqua, *et al.*, pH-dependent binding engineering reveals an FcRn affinity threshold that governs IgG recycling, *J. Biol. Chem.*, 2015, **290**(7), 4282–4290.

18 A. Grevys, M. Bern, S. Foss, D. B. Bratlie, A. Moen, K. S. Gunnarsen, *et al.*, Fc engineering of human IgG1 for altered binding to the neonatal Fc receptor affects Fc effector functions, *J. Immunol.*, 2015, **194**(11), 5497–5508.

19 M. H. G. Fonseca, G. P. Furtado, M. R. L. Bezerra, L. Q. Pontes and C. F. C. Fernandes, Boosting half-life and effector functions of therapeutic antibodies by Fc-engineering: An interaction-function review, *Int. J. Biol. Macromol.*, 2018, **119**, 306–311.

20 J. K. Kim, M. Firan, C. G. Radu, C. H. Kim, V. Ghetie and E. S. Ward, Mapping the site on human IgG for binding of the MHC class I-related receptor, FcRn, *Eur. J. Immunol.*, 1999, **29**(9), 2819–2825.

21 C. Medesan, D. Matesoi, C. Radu, V. Ghetie and E. S. Ward, Delineation of the amino acid residues involved in transcytosis and catabolism of mouse IgG1, *J. Immunol.*, 1997, **158**(5), 2211–2217.

22 S. Popov, J. G. Hubbard, J. Kim, B. Ober, V. Ghetie and E. S. Ward, The stoichiometry and affinity of the interaction of murine Fc fragments with the MHC class I-related receptor, FcRn, *Mol. Immunol.*, 1996, **33**(6), 521–530.

23 A. Šali and T. L. Blundell, Comparative protein modelling by satisfaction of spatial restraints, *J. Mol. Biol.*, 1993, **234**(3), 779–815.

24 D. A. Case, I. Y. Ben-Shalom, S. R. Brozell, D. S. Cerutti, T. E. Cheatham III, V. W. D. Cruzeiro, *et al.*, *AMBER 2018*, University of California, San Francisco, 2018.

25 V. Hornak, R. Abel, A. Okur, B. Strockbine, A. Roitberg and C. Simmerling, Comparison of multiple Amber force fields and development of improved protein backbone parameters, *Proteins: Struct., Funct., Bioinf.*, 2006, **65**(3), 712–725.

26 J. A. Izaguirre, D. P. Catarello, J. M. Wozniak and R. D. Skeel, Langevin stabilization of molecular dynamics, *J. Chem. Phys.*, 2001, **114**(5), 2090–2098.

27 Y. Meng and A. E. Roitberg, Constant pH replica exchange molecular dynamics in biomolecules using a discrete protonation model, *J. Chem. Theory Comput.*, 2010, **6**(4), 1401–1412.

28 S. L. Williams, C. A. F. De Oliveira and J. A. McCammon, Coupling constant pH molecular dynamics with accelerated molecular dynamics, *J. Chem. Theory Comput.*, 2010, **6**(2), 560–568.

29 J. P. Ryckaert, G. Ciccotti and H. J. Berendsen, Numerical integration of the cartesian equations of motion of a system with constraints: molecular dynamics of n-alkanes, *J. Comput. Phys.*, 1977, **23**(3), 327–341.

30 M. Feig, J. Karanicolas and C. L. Brooks III, *MMTSB tool set. MMTSB NIH Research Resource*, The Scripps Research Institute, La Jolla, CA, 2001.

31 D. R. Roe and T. E. Cheatham III, PTRAJ and CPPTRAJ: software for processing and analysis of molecular dynamics trajectory data, *J. Chem. Theory Comput.*, 2013, **9**(7), 3084–3095.

32 B. R. Brooks, D. Janežič and M. Karplus, Harmonic analysis of large systems. I Methodology, *J. Comput. Chem.*, 1995, **16**(12), 1522–1542.

33 A. Onufriev, D. Bashford and D. A. Case, Exploring protein native states and large-scale conformational changes with a modified generalized born model, *Proteins: Struct., Funct., Bioinf.*, 2004, **55**(2), 383–394.

34 J. Weiser, P. S. Shenkin and W. C. Still, Approximate atomic surfaces from linear combinations of pairwise overlaps (LCPO), *J. Comput. Chem.*, 1999, **20**(2), 217–230.

35 E. Krissinel and K. Henrick, Inference of macromolecular assemblies from crystalline state, *J. Mol. Biol.*, 2007, **372**(3), 774–797.

36 M. Petukh, L. Dai and E. Alexov, SAAMBE: webserver to predict the charge of binding free energy caused by amino acids mutations, *Int. J. Mol. Sci.*, 2016, **17**(4), 547.

37 W. L. DeLano, *The PyMOL molecular graphics system*, DeLano Scientific LLC, San Carlos, CA, USA, 2003.

38 L. Wang, M. Zhang and E. Alexov, DelPhiPKa web server: predicting pK_a of proteins, RNAs and DNAs, *Bioinformatics*, 2015, **32**(4), 614–615.

39 C. Monnet, S. Jorieux, N. Souyris, O. Zaki, A. Jacquet, N. Fournier, *et al.*, Combined glyco-and protein-Fc engineering simultaneously enhance cytotoxicity and half-life of a therapeutic antibody, *mAbs*, 2014, **6**(2), 422–436.

40 C. Wang, Y. Wu, L. Wang, B. Hong, Y. Jin, D. Hu, *et al.*, Engineered soluble monomeric IgG1 Fc with significantly

decreased non-specific binding, *Front. Immunol.*, 2017, **8**, 1545.

41 Y. A. Yeung, M. K. Leabman, J. S. Marvin, J. Qiu, C. W. Adams, S. Lien, *et al.*, Engineering human IgG1 affinity to human neonatal Fc receptor: impact of affinity improvement on pharmacokinetics in primates, *J. Immunol.*, 2009, **182**(12), 7663–7671.

42 T. Ying, W. Chen, R. Gong, Y. Feng and D. S. Dimitrov, Soluble monomeric IgG1 Fc, *J. Biol. Chem.*, 2012, **287**(23), 19399–19408.

43 T. Ying, T. Ju, Y. Wang, P. Prabakaran and D. Dimitrov, Interactions of IgG1 CH_2 and CH_3 Domains with FcRn, *Front. Immunol.*, 2014, **5**, 146.

44 J. K. Kim, M. F. Tsen, V. Ghetie and E. S. Ward, Localization of the site of the murine IgG1 molecule that is involved in binding to the murine intestinal Fc receptor, *Eur. J. Immunol.*, 1994, **24**, 2429–2434.

45 D. C. Roopenian, G. J. Christianson, T. J. Sproule, A. C. Brown, S. Akilesh, N. Jung, *et al.*, The MHC class I-like IgG receptor controls perinatal IgG transport, IgG homeostasis, and fate of IgG-Fc-coupled drugs, *J. Immunol.*, 2003, **170**(7), 3528–3533.

46 B. T. Walters, P. F. Jensen, V. Larraillet, K. Lin, T. Patapoff, T. Schlothauer, *et al.*, Conformational destabilization of immunoglobulin G increases the low pH binding affinity with the neonatal Fc receptor, *J. Biol. Chem.*, 2016, **291**(4), 1817–1825.

47 S. P. Edgcomb and K. P. Murphy, Variability in the pK_a of histidine side-chains correlates with burial within proteins, *Proteins: Struct., Funct., Bioinf.*, 2002, **49**(1), 1–6.

48 W. T. Chu, Y. J. Wu, J. L. Zhang, Q. C. Zheng, L. Chen, Q. Xue, *et al.*, Constant pH Molecular Dynamics (CpHMD) and mutation studies: insights into AaegOBP1 pH-induced ligand releasing mechanism, *J. Proteins Proteomics*, 2012, **1824**(7), 913–918.

49 W. T. Chu, J. L. Zhang, Q. C. Zheng, L. Chen, Y. J. Wu, Q. Xue, *et al.*, Constant pH molecular dynamics (CpHMD) and molecular docking studies of CquiOBP1 pH-induced ligand releasing mechanism, *J. Mol. Model.*, 2013, **19**(3), 1301–1309.